



ARTICLE

Study on the Durability of Recycled Powder Concrete against Sulfate Attack under Partial Immersion Condition

Hualei Bai^{1,2}, Ying Li^{1,2,*} and Dahu Dai^{1,2}

¹School of Civil Engineering, Qinghai University, Xining, 810016, China

²Qinghai Provincial Key Laboratory of Energy Saving Building Materials and Engineering Safety, Xining, 810016, China

*Corresponding Author: Ying Li. Email: liying.qh@163.com

Received: 06 November 2021 Accepted: 24 January 2022

ABSTRACT

In order to make full use of waste recycled fine powder (RFP) in concrete and achieve the goal of carbon neutrality in the concrete industry, the durability of sulfate resistance is an important aspect of evaluating the performance of recycled powder concrete (RPC). Therefore, the durability of RPC under partial sulfate immersion was studied to provide theoretical guidance for understanding the erosion mechanism of RPC. The compressive strength, mass loss, and microstructure change patterns of RPC under partial immersion of 5% Na₂SO₄ and MgSO₄ solutions were analyzed by cubic compressive strength, mass loss rate, SEM-EDS, and XRD. The results showed that the surface crystalline matter of concrete in Na₂SO₄ solution was mainly white powders, and that of concrete in MgSO₄ solution was mainly transparent paste, both of which had a little spalling on the outer surface of the concrete. The compressive strength and mass loss rate of concrete with 20% RFP was relatively good, indicating that concrete with 20% RFP had better durability against sulfate. The compressive strength of the lower part of the concrete partially immersed in Na₂SO₄ solution was higher than that of the upper part and the strength of the lower part of RPC-2 was 3.11% higher than the upper part at 180 d; The pattern was reversed in the MgSO₄ solution, where the strength of the lower part of RPC-2 was 19.74% lower than the upper part at 180 d. Microscopic analysis showed that the hydration products of RPC were mainly gypsum and ettringite, while the RPC produced more hydration products with the promotion of magnesium ion in the MgSO₄ solution. The higher the replacement rate of RFP, the more frequent the gypsum-type failures in the concrete.

KEYWORDS

Recycled powder concrete; recycled fine powder; sulfate resistance; compressive strength

1 Introduction

With urbanization in China, much construction waste has been produced from new constructions, reconstructions, and demolitions. In order to mitigate the impact of randomly dumped construction waste on the environment, scholars have attempted using construction waste as recycled coarse aggregate and recycled fine aggregate in the place of natural stone and sand to produce concrete materials. To some extent, construction waste pollution of the environment was reduced, and the shortage of natural sand, stone, and other raw materials for concrete was alleviated. Meanwhile, some scholars tried to use other new cementitious materials instead of traditional cementitious composites to reduce environmental



pollution. Zhang et al. [1] investigated the effects of PVA fibers and nano-SiO₂ on the mechanical properties of modified earth aggregates. Gao et al. [2] found that PVA fibers and nano-SiO₂ could significantly improve the bonding properties of concrete specimens. However, while producing the recycled aggregates, a large amount of fine powder with particle size below 0.075 mm is generated, i.e., the recycled fine powder (RFP). It has been shown that RFP has certain activities and can be used as a mineral admixture to replace cement in concrete [3–5]. Preparing recycled powder concrete (RPC) with RFP could improve the utilization rate of construction waste and save cement, which in turn reduces CO₂ emissions and helps achieve carbon neutrality in the cement industry.

Scholars have researched the basic properties of recycled aggregates and RFP. However, the research on recycled aggregates was not without limitations, and the performances of recycled aggregates were evaluated by comparing the concrete containing recycled aggregates with that containing natural aggregates [6]. Later, scholars successfully applied recycled aggregates to actual highway subgrades [7–9]. Li et al. [10] studied the durability of recycled aggregate concrete under the coupling effect of freeze-thaw and sulfate and found that the resistance increased with the increase of recycled concrete aggregate content. Wang et al. [11] discussed the methods and principles of improving the performance of recycled coarse aggregate concrete. In contrast, the research on RFP with higher fineness and activity is relatively lacking. It is found that replacing cement with a small amount of RFP could reduce the compressive strength of concrete but had a positive effect on flexural and tensile splitting properties [12,13]. Tang et al. [14] studied the performance of RFP in self-compacting concrete and found that RFP as an admixture could completely replace fly ash. Oksri-Nelfia et al. [15] used ground waste concrete powder to replace about 25% of polyester cement, and the properties of the prepared concrete were not affected. Most of the existing studies focused on the effect of RFP replacement rate on the mechanical properties of RPC, and it was found that the RFP as an admixture into the concrete can still maintain good mechanical properties. However, there are relatively few experimental studies on the durability of RPC. Research on the durability of RPC against sulfate erosion is almost blank. Since the resistance to sulfate erosion is an essential aspect of concrete durability, the durability of RPC is also extremely important.

As the saline land in Qinghai is rich in sulfate, concrete structures built there are subjected to long-term sulfate erosion that could affect their strength and durability. The applicability of RPC in saline lands depends on its durability against sulfate attack, and the sulfate deterioration mechanism of RPC needs to be investigated urgently. However, the durability against sulfate attack is a complex problem concerning the reaction between SO₄²⁻ and cement hydration products that cause chemical attacks, the diffusion of ions, physical crystallization, and other processes. The main deterioration mechanisms of normal concrete are crystalline salt erosion [16], gypsum type erosion [17,18], ettringite erosion [19], and lagging ettringite carbon-sulfur calcium silicate erosion [20,21]. Liu et al. [22] found that chemical erosion occurred mainly in concrete under sulfate attacks. Zhang et al. [23] conducted accelerated indoor tests and found that chemical-physical coupled erosion in concrete occurred under dry and wet cycles. Komljenovic et al. [24] found that alkali-activated slag had better sulfate resistance. Guo et al. [25] concluded that layered double hydroxides were beneficial to concrete durability against sulfate. Nehdi et al. [26] analyzed the erosion mechanism of concrete under full immersion conditions. Their study found that carbonation was the prerequisite for the destruction of sulfate crystals, after which sulfate crystals occurred on the carbonized surface while the interior of the concrete underwent chemical attacks. In addition, semi-immersed concrete does not manifest the wick effect of porous materials. Wu et al. [27] studied sulfate erosion at 5°C and found that MgSO₄ is more likely to form indirectly in MgSO₄ solution, while MgSO₄ forms directly in Na₂SO₄ solution through erosion products. Therefore, it is necessary to study whether RPC has the same erosion mechanism as ordinary concrete.

Since replacing cement with industrial waste fly ash is currently the most common process, scholars have investigated the sulfate resistance mechanism of concrete with fly ash under sulfate immersion

[28,29]. Nie et al. [30] numerically simulated concrete with fly ash and found that fly ash's pozzolanic effect and hydration reaction effectively resisted sulfate erosion. Deng et al. [31] found that adding fly ash to concrete could change the aluminum phase and promote ettringite formation. Džunuzović et al. [32] found that concrete with a low Si/Al ratio had high sulfate resistance. Jiang et al. [33] found that high belite cement commonly used in hydraulic concrete had magnesium hydroxide formed on its surface, which was favorable to MgSO_4 erosion. Thus, adding fly ash had good resistance to Na_2SO_4 and MgSO_4 erosion.

To sum up, mineral admixtures such as fly ash and slag could improve concrete's resistance to sulfate erosion. Since RFP has similar properties as fly ash, whether RPC has the same durability under sulfate erosion is worth investigating. In order to explore the effects of RPC under sulfate erosion, partial sulfate immersion tests were conducted on RPC. The effects of different replacement rates, sulfate types, and immersion times on the mechanical properties of RPC were investigated. The mechanism of RPC's durability against sulfate attack was expounded. Compared with ordinary concrete, the optimum content of RPC under partial sulfate immersion was obtained.

2 Experimental Program

2.1 Materials

RFP was produced by crushing waste concrete beams in the laboratory, and the strength of the concrete was measured at around 30 MPa with a rebound tester. Firstly, the concrete beams were crushed manually and by a crusher to obtain fine aggregate. Then, the fine aggregate was transferred into a ball mill for 30 min ball milling. The ball-milled product was sieved through a 0.075 mm sieve to obtain RFP. The chemical composition of cement and RFP are shown in Table 1. The results of the XRD diffraction analysis of RFP are shown in Fig. 1. The SiO_2 diffraction peaks are higher, mainly because the RCP contains a large amount of sand and gravel debris. The particle size distribution of RFP is shown in Fig. 2 [34]. Besides, P.O42.5 cement, coarse aggregate with particle sizes ranging from 4.75 to 20 mm, natural sand with a fineness modulus of 3.02 was also used in this study.

Table 1: Chemical composition of raw minerals (%)

Raw materials	CaO	SiO ₂	Al ₂ O ₃	Fe ₂ O ₃	MgO	SO ₃	Na ₂ O	CO ₂	TiO ₂	K ₂ O
Cement	67.7	12.0	3.02	6.77	0.09	2.37	0.01	6.12	0.56	0.68
RFP	34.5	25.8	4.44	6.04	0.15	0.44	0.06	25.8	0.65	1.06

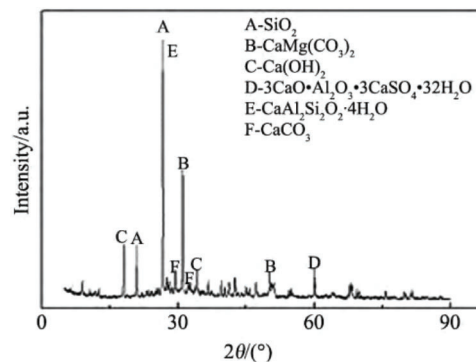


Figure 1: XRD diffraction pattern of RFP

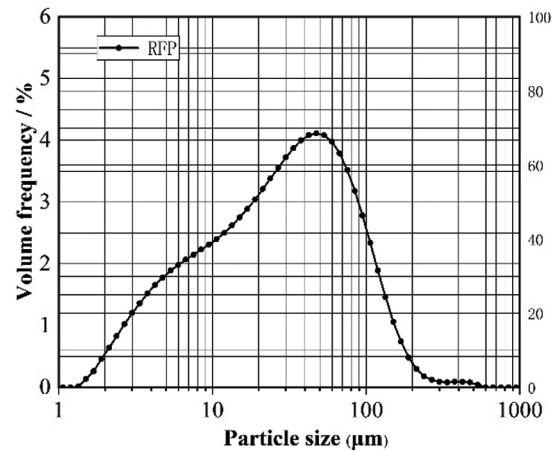


Figure 2: Particle size distribution of RFP

2.2 Experiment Methods

According to the mixing ratio in Table 2, 0%, 10%, 20%, 30%, and 40% RFP were used to replace the cement and make three prismatic test blocks of 100 mm × 100 mm × 400 mm. A group of 3 pieces was used for comparison, and a total of 105 pieces of prismatic concrete were produced. Some samples are shown in Fig. 3. The casted test blocks were kept at room temperature for 24 h before removing the molds. The test blocks were placed in a standard curing room for 28 d. Afterward, the test blocks were removed from the curing room and dried naturally for 2 d. The blocks were weighed, and the weights were recorded as the original masses. Then, the test blocks were placed into 5% Na₂SO₄ and MgSO₄ solution, exactly half immersed. Since most concrete components are often semi-buried or semi-immersed in an underground sulfate environment, in order to simulate this actual engineering environment, a half immersion method was adopted to study the durability of RPC. The partial immersion at room temperature was maintained for 30, 60, 90, 120, 150, and 180 d. Afterward, the test blocks were taken out and dried naturally for 2 d before weighing them again. For each immersion period, 45 pieces of the test blocks were cut into equal cubes of 100 mm × 100 mm × 100 mm, as shown in Fig. 4. The compressive strength of the concrete cubes was measured according to the Chinese Standard for Test Methods of Concrete Physical and Mechanical Properties (GB/T 50081-2019) [35].

Table 2: The mixture ratio of concrete

No.	RFP (%)	W/C	Cement (kg)	RFP (kg)	Stone (kg)	Sand (kg)	Water (ml)	Water-reducers (%)	Slump (mm)
NC-0	0	0.45	455	0	1032	595	205		55
RPC-1	10	0.45	410	46	1032	595	205		60
RPC-2	20	0.45	364	91	1032	595	205	0.5	58
RPC-3	30	0.45	319	137	1032	595	205		56
RPC-4	40	0.45	273	182	1032	595	205		55



Figure 3: 100 mm × 100 mm × 400 mm sample diagram

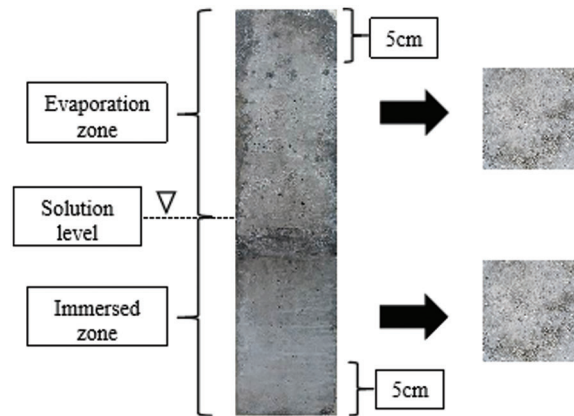


Figure 4: Sampling schematic

After the immersion, the concrete surface was desalinated, and the weight was measured after drying naturally for 2 d. The mass-loss rate of the concrete Δm was determined according to the following equation:

$$\Delta m = \frac{m_{28} - m_r}{m_{28}} \times 100\%$$

where m_r is the mass of the eroded concrete on day r ; m_{28} is the mass of the concrete before immersion.

After the destruction, two cube concrete test blocks were taken from the same position, and a total of six of each group were taken and put into the analysis of pure alcohol to stop hydration. Changes in the microstructural composition of the samples were tested using SEM-EDS and XRD. The sample soaked in the analysis of pure alcohol was taken out and dried in an oven at 80°C for 6 h. Three of the damaged samples in each group were tested by SEM-EDS (JSM-5610LV) to observe the characteristics of the hydration products and erosion products. EDS energy spectrum was used to analyze the element types and contents of the samples, and SEM images were used to qualitatively analyze the erosion products. The other 3 damaged samples in each group were ground using a grinder, and the crystal phase of the concrete was analyzed using an X-ray instrument (Rigaku D/MAX 2500PC) to observe the hydration products and the microstructure composition of the upper and lower parts of the RPC during immersion.

3 Result and Discussion

3.1 Morphology Analysis

The changes in RPC morphology after partial immersion in sulfate solution for 180 d are shown in Figs. 5 and 6. Under partial immersion in Na_2SO_4 solution, many white crystals appear on the upper part of the concrete. The peeling of NC-0 is not apparent, and the cement paste on the surface of RPC-4 peels off partially. With the increase of RFP content, the flaking of the middle part increases gradually and the sulfate crystallization appears on the bottom surface. The surface crystalline morphology of RPC changes with the increase of immersion time, and the crystallization process is generally divided into three stages. In the early stage, long crystals formed at the middle part of the concrete. The concrete sample was intact, and the crystal area was about 5 mm from the solution. In the middle stage, the middle part of the concrete crystallized from fiber length to powder. Due to the evaporation and absorption of water [36,37], a high concentration zone formed on the liquid surface, and Na_2SO_4 gradually crystallized on the concrete surface. In the late stage, the crystalline state was in the cross-distribution of powder and flocculation, and the surface of the RPC was partially peeled off at the crystalline position above the liquid level.



Figure 5: Corrosion morphology of RPC in Na_2SO_4 solution
 Note: The replacement rate is 0%, 10%, 20%, 30%, and 40% from left to right.



Figure 6: Corrosion morphology of RPC in MgSO_4 solution
 Note: The replacement rate is 0%, 10%, 20%, 30%, and 40% from left to right.

Fig. 6 shows the concrete morphology after being eroded by MgSO_4 for 180 d. A large number of paste-like viscous salt crystals appeared near the liquid level of the concrete. After removing the viscous material, the surface of the samples showed spalling spots, and the number of spots increased gradually with the increase of the RFP content. In the process of MgSO_4 solution eroding, viscous crystals formed gradually. At the liquid level, a high concentration zone of MgSO_4 was formed. After the concentration gradient, the ions diffused and migrated to the upper part of the concrete. In summary, it can be seen that the main difference in the morphology of the concrete after erosion by Na_2SO_4 and MgSO_4 solutions is the crystal shape and the spalling position. The surface morphology of concrete in Na_2SO_4 solution is dominated by white powdery crystals, while transparent paste-like crystals dominate the surface morphology of concrete in MgSO_4 solution. After removing the crystalline salt on the concrete surface, it can be found that the surface spalling of the middle and upper part of concrete after Na_2SO_4 erosion was more severe, while the lower part of concrete after MgSO_4 erosion showed sporadic spalling and the middle and upper part was intact.

3.2 Cube Compressive Strength Analysis

The concrete test blocks of the upper and lower parts were subjected to a cubic compressive strength test. Fig. 7a shows the compressive strength variation pattern of the upper part with immersion time in the Na_2SO_4 solution. The general compressive strength of the control group (NC-0) increased with immersion time. The high concentration zone of Na_2SO_4 is in the middle part of ordinary concrete immersed in the Na_2SO_4 solution. After the concentration gradient effect, it gradually extended to the upper concrete and formed a small number of erosion products (gypsum and ettringite) to fill the concrete, which resulted in the strength enhancement of the upper part [38]. The compressive strength of concrete in the upper part at 180 d was 46.69 MPa, indicating that ordinary concrete had good durability against sulfate. With the increase of time, the compressive strength of RPC increased gradually. RPC has obvious peaks at 90 d, with the peaks of RPC-1, RPC-2, RPC-3, and RPC-4 being 43.6, 42.98, 41.74, 36.64 MPa, respectively. After 180 d of immersion, RPC-2 had the highest compressive strength of 43.03 MPa, which was 3.67 MPa lower than NC-0. The results showed that RPC could produce secondary hydration, pozzolanic effect, and filling effect of sulfate attack products, which could enhance the early strength of RPC. In the late immersion stage, the RFP refines the pore size and the filling effect of the Na_2SO_4 erosion product (ettringite), further enhancing the late strength of RPC-2 with 20% RFP. Morphology analysis indicated that with the increase of RFP replacement rate, increasingly larger surface layers fall off the concrete, while the compressive strength remained unchanged. Therefore, the inner concrete core was not significantly affected, and the later strength was stronger than the initial strength.

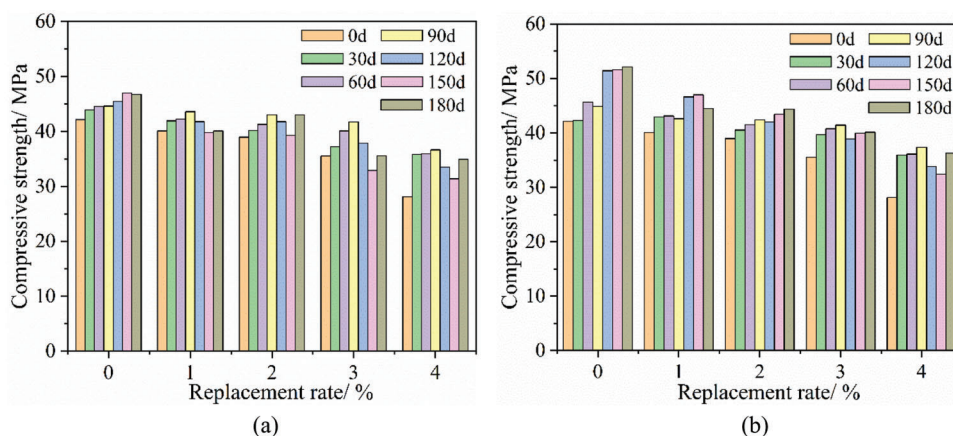


Figure 7: Compressive strength variation of the concrete in Na_2SO_4 solution

Fig. 7b shows the histogram of compressive strength in the lower part of the concrete with time under partial Na_2SO_4 immersion. The compressive strength of NC-0 gradually increased with immersion time, reaching 52.14 MPa at 180 d. Moreover, the compressive strength in the lower part of ordinary concrete at 180 d was 5.45 MPa higher than that of the upper part, and more corrosion products formed in ordinary concrete because the lower part was fully immersed. With immersion time below 90 d, the compressive strength in the lower part of RPC gradually increased with time. The compressive strengths of RPC-3 and RPC-4 were 41.44 and 37.34 MPa at 90 d. The peak compressive strength in the lower part of the concrete appeared slightly different in time. The peak compressive strength in the concrete with 10% and 30% RFP appeared at 120 d. However, the peak compressive strength in the concrete with 20% and 40% RFP appeared at 90 and 150 d, respectively. After 180 d of immersion, the compressive strength of the concrete with 10% RFP decreased to 44.48 MPa, and that of the concrete with 20% RFP increased further to 44.37 MPa. The compressive strength could reach about 85% of the blank group, and the RPC was not yet damaged by erosion. At the same time, the strength of the lower part of RPC-2 was 3.11% higher than the upper part concrete at 180 d. When RPC was corroded by the Na_2SO_4 solution, the peak compressive strength in the lower part of the concrete with different RFP replacement rates was higher than that of the upper part, indicating that the upper part of RPC was more seriously affected by the partial immersion in Na_2SO_4 . These results are consistent with those of other scholars [39]. Na_2SO_4 had a positive effect on the increase of concrete strength under short-term partial immersion, and RPC had the properties of ordinary concrete, especially those with the RFP replacement rate of 20% (RPC-2), which showed excellent resistance to Na_2SO_4 erosion. The results showed that the infiltration of erosion products (ettringite and gypsum) produced by Na_2SO_4 could fill the pores of the concrete [40,41] and reduce their size, and the recycled micro-powder could refine the pore size, thus improving the compressive strength of the concrete.

Fig. 8a shows the variation of compressive strength with time in the upper part of the concrete immersed in MgSO_4 . The compressive strength of NC-0 increased to 52.46 MPa at 180 d. With different RFP replacement rates, the compressive strength of RPC showed different changing patterns. At 180 d, the compressive strength of RPC-1, RPC-2, RPC-3, and RPC-4 decreased to 39.95, 43.7, 35.29, and 29.56 MPa, respectively. However, the compressive strength of RPC-2 reached 83.3% of that of NC-0. The compressive strength in the upper part of the concrete immersed in the MgSO_4 solution was higher than that immersed in the Na_2SO_4 solution, indicating that the upper part of the concrete was corroded more seriously in the Na_2SO_4 environment. These results are consistent with the findings by [42]. In the early immersion stage, Mg^{2+} could increase the compressive strength under the action of RFP.

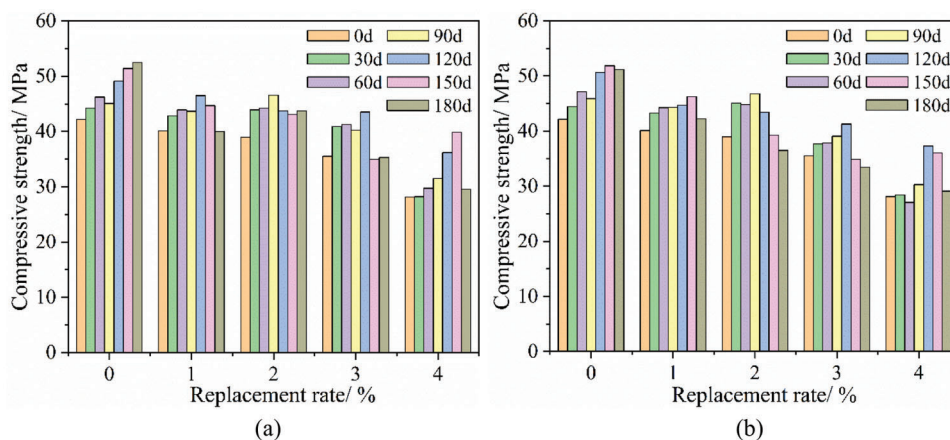


Figure 8: Compressive strength variation of concrete in MgSO_4 solution

Fig. 8b shows the variation of compressive strength in the lower part of the concrete immersed in $MgSO_4$ solution. Under $MgSO_4$ erosion, ordinary concrete (NC-0) showed the peak compressive strength of 51.87 MPa at 150 d. At 180 d, the compressive strength of NC-0 is 51.16 MPa, which was 1.3 MPa lower than the strength of the upper part of the concrete. When immersed in $MgSO_4$ solution, the compressive strength of RPC-1, RPC-2, RPC-3, and RPC-4 peaked at 46.26, 46.75, 41.27, and 37.27 MPa at 150, 90, 120, and 120 d, respectively. The main reason is that as the number of RFP increases, the pores of the concrete are filled, the erosion products (ettringite) increase simultaneously, and the superimposed effect increases the strength of the concrete. At 180 d, the compressive strength in the lower part of RPC with 10%, 20%, 30%, and 40% RFP decreased to 42.2, 36.5, 33.42, and 29.1 MPa, respectively, and the strength of the upper part of RPC-2 was 7.2 MPa higher than the lower part after 180 d of 5% $MgSO_4$ erosion. The compressive strength of RPC-4 decreased to about 56.7% of that of NC-0, while that of RPC-2 was 71% of that of NC-0. Therefore, the RPC with 20% RFP had good durability. The intrinsic factor may be the hydration reaction of part of the RFP, which reduces the internal C_3A content and thus achieves the sulfate resistance. Under $MgSO_4$ erosion, the compressive strength in the upper part of RPC with RFP replacement rates over 10% was higher than that in the lower part. The reason for the lower compressive strength in the lower part of the concrete immersed in Na_2SO_4 might be due to the chemical erosion by $MgSO_4$ that produced ettringite and gypsum and the reaction between Mg^{2+} and C-S-H that produced gypsum and ettringite. At the same time, pH was reduced, which was beneficial to the formation of gypsum [43].

To sum up, whether in Na_2SO_4 solution or $MgSO_4$ solution, with the increase of RFP, RPC showed a gradual decrease in resistance to sulfate erosion performance. The reason is that when the amount of RFP is small, the particles of RFP are finer, and its secondary hydration effect is obvious. With the further increase of the RFP admixture, the cement content decreases, and the secondary hydration effect of the RFP inside the concrete is difficult to reach the effect of cement hydration. However, the RPC has better resistance to sulfate erosion when the RFP is blended at 20%, due to its total internal porosity and secondary hydration can better resist sulfate erosion [34].

3.3 Quality Loss Rate Analysis

Fig. 9 shows the variation pattern of mass loss rate with time in RPC immersed in Na_2SO_4 solution. The mass-loss of RPC is affected by the increase of corrosion products and the surface peeling of concrete. The mass loss rate variation of NC-0 is similar to that of RPC with 10% RFP. The mass-loss rates of NC-0 and RPC-1 at 180 d are 0.209% and 0.364%, while that of concrete with 20%, 30%, and 40% RFP are 0%, 0.83%, and 0.627%. The mass-rate of RPC-2 showed a similar pattern to RPC-3. The mass of RPC-4 with 40% RFP kept decreasing from 90 d, indicating that the corrosion by Na_2SO_4 intensified as the RFP content exceeded a certain amount. Due to the high solubility of Na_2SO_4 on the concrete surface, the high concentration of Na_2SO_4 diffuses and gradually invades the interior, producing erosion products (gypsum and ettringite) in the surface layer. As the porosity of the surface layer decreased, the infiltration of Na_2SO_4 was reduced, and the excessive Na_2SO_4 physically crystallized on the surface. With the accumulation of ettringite and gypsum on the concrete surface, the pressure inside the pores increased. Over time, the corrosion products inside the concrete increase, filling the pores and communicating apertures. The mass of RPC-2 remained relatively stable during the immersion, and the increase at 90 d may be due to the large number of erosion products produced inside the concrete, filling the internal pores.

Fig. 10 shows the mass-loss rate variation of concrete immersed in $MgSO_4$ solution. The mass-loss rates of NC-0 and RPC-1, RPC-2, RPC-3, and RPC-4 at 180 d were 0.34%, 0.2%, 0.143%, 0.73%, and 0.792%, respectively. The mass of NC-0 and RPC all reduced. The mass-loss rate increased with the increase of RFP content, which may be attributed to the lower rate of erosion product accumulation and the higher rate of surface peeling. With the increase of RFP content, the pores inside the concrete were refined, which

decreased the solution absorption. Secondly, a viscous protective film formed on the concrete surface under the erosion of MgSO_4 , which slowed down the solution immersion. As Ca^{2+} precipitated from C-S-H [44], the pH of the concrete decreased, which was more favorable to cause internal damage and mass loss to the concrete. When the RFP content exceeded 30%, the mass loss became more severe.

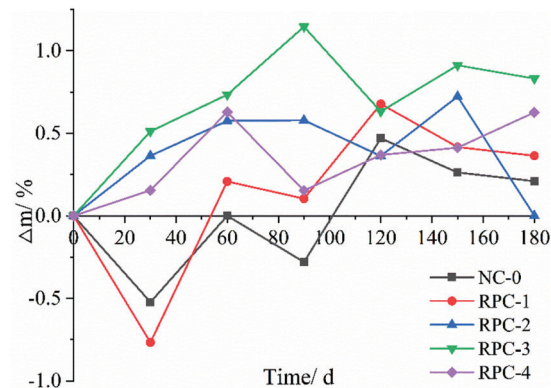


Figure 9: Mass loss rate variation of concrete in Na_2SO_4 solution

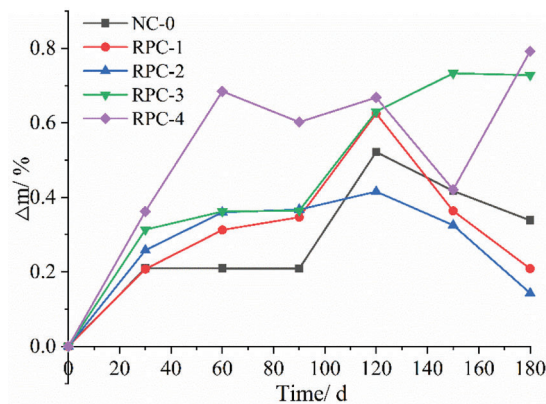


Figure 10: Mass loss rate variation of concrete in MgSO_4 solution

3.4 XRD Analysis of Surface Peeling

After the 180 d immersion in Na_2SO_4 , the powder crystalline products on the middle surface of the concrete sample were collected and analyzed using XRD. After 180 d of immersion in MgSO_4 solution, the viscous matter on the middle surface of the concrete was collected with a knife and analyzed using XRD. As shown in Fig. 11, Na_2SO_4 crystals are the main salt precipitates in the middle of the samples soaked in the Na_2SO_4 solution, while $\text{MgSO}_4 \cdot 6\text{H}_2\text{O}$ is the main salt precipitates in the middle of the samples soaked in the MgSO_4 solution.

3.5 SEM-EDS Analysis of the Samples under Na_2SO_4 Attack

SEM was adopted to study the morphological characteristics of the concrete after 180 d of Na_2SO_4 erosion and the erosion mechanism of RPC. SEM images of the upper and lower parts of NC-0, RPC-2, and RPC-4 after the 180 d immersion in Na_2SO_4 solution are shown in Fig. 12. The main reactions between Na_2SO_4 and concrete are as follows:

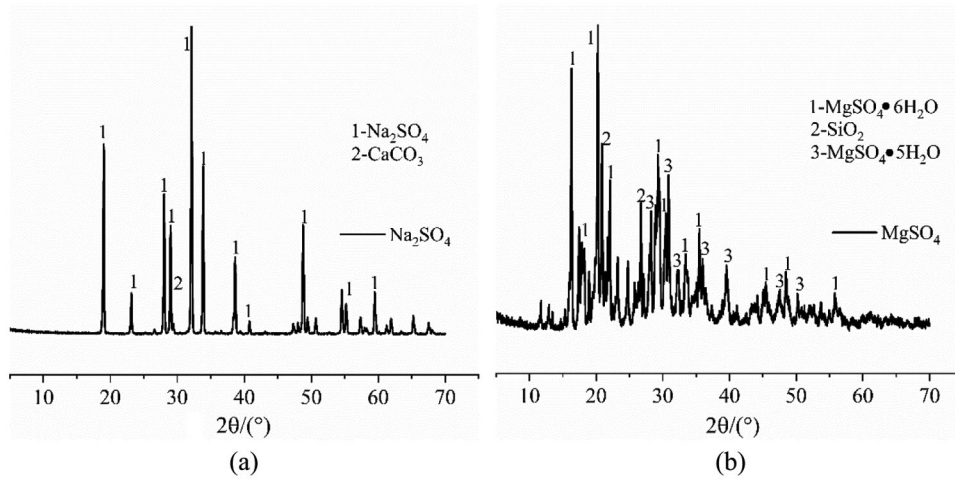


Figure 11: XRD spectrum of concrete surface precipitates

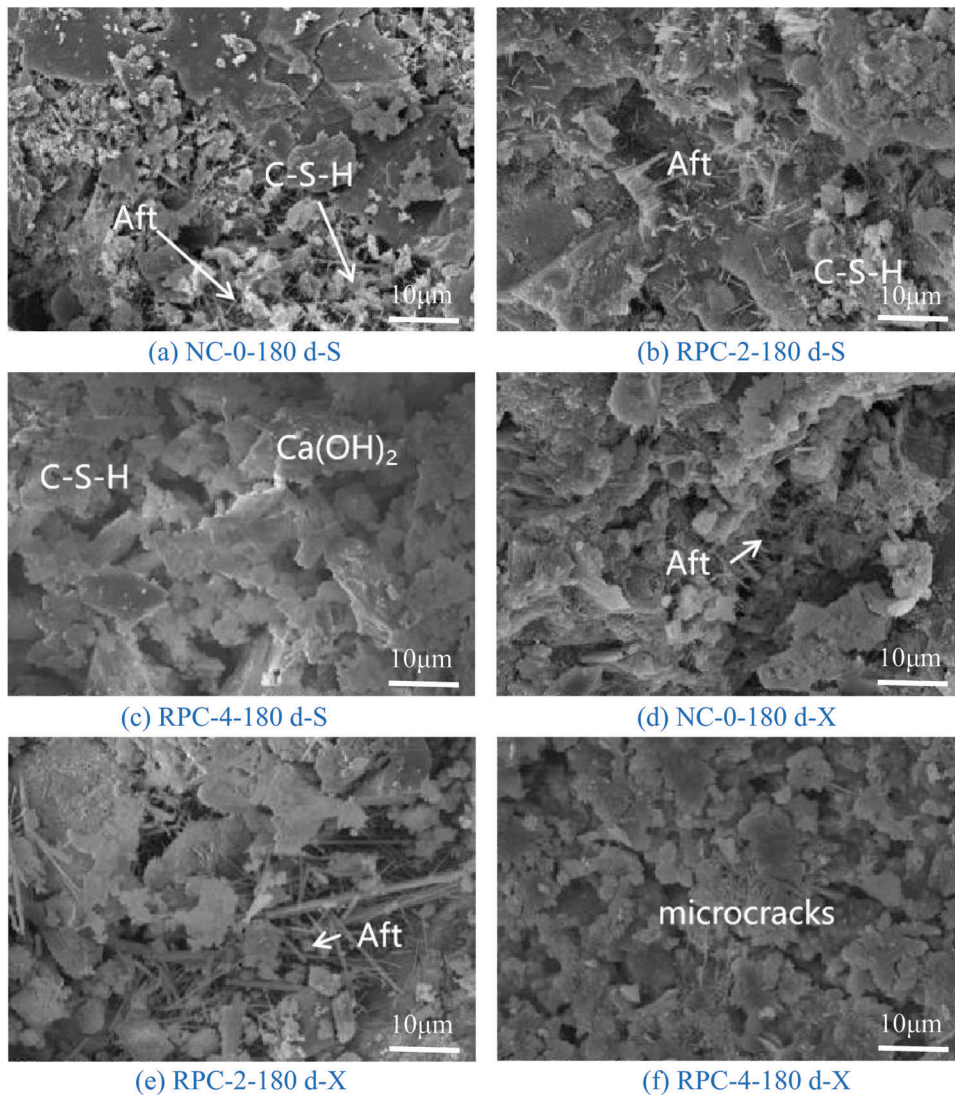
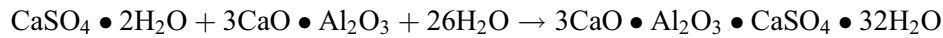
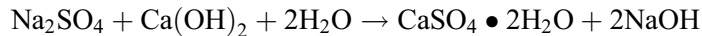


Figure 12: SEM diagram of concrete with different RFP replacement rates $\times 2000$ times



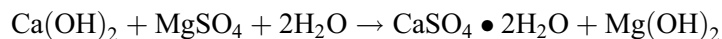
Na_2SO_4 reacts with the concrete to form gypsum ($\text{CaSO}_4 \cdot 2\text{H}_2\text{O}$) and ettringite ($3\text{CaO} \cdot \text{Al}_2\text{O}_3 \cdot \text{CaSO}_4 \cdot 32\text{H}_2\text{O}$, AFt).

In Fig. 12, hydration products can be observed in the NC-0 concrete microstructure, including massive gypsum, needle-rod-like ettringite, gel products, and some scattered particles in the upper part, which may be the crystallization of Na_2SO_4 . Compared with NC-0, the concrete with 20% RFP has many needle-stick and blocky crystals. In particular, the lower part of RPC-2 is rich in needle-rod-like ettringite. Therefore, the compressive strength in the lower part of RPC-2 is higher than that of the upper part because of the higher amount of corrosion and hydration products. The microstructure diagrams of the upper and lower parts of RPC-4 show that the upper part of the concrete has a large amount of CH, gypsum, and flocculent C-S-H. Obvious cracks are observed in the lower part of RPC-2, and CH, AFt, and scattered granular materials are observed around the cracks. The scattered granular material may be thenardite, indicating the predominant chemical erosion inside the concrete. In contrast, the concrete with 40% RFP shows mainly flocculent and lumpy crystals. These results show that with the increase of the RFP content, the needle and rod crystals inside the concrete decrease, but the lumpy crystals increase.

Fig. 13 shows the EDS of concrete. In the energy spectrum of RPC-2 after the 180 d immersion in Na_2SO_4 , the main elements in the upper part are Si, Ca, O, and Al, which may be C-S-H, C-A-H, and AFm. In the lower part of the diagram, more marked Ca and O elements are observed, and the marked O elements are significantly increased. In addition to the small amount of Mg elements, the calibrated substances may have produced AFm [22]. Therefore, Na_2SO_4 was consumed initially to produce monosulfide sulfoaluminate. The average temperature in Xining, Qinghai Province is between -1°C and 15°C throughout the year, which is favorable for the production of the AFm phase.

3.6 SEM-EDS Analysis of Samples under MgSO_4 Attack

Fig. 14 shows the SEM image of concrete after 180 d of partial immersion in MgSO_4 . The main chemical erosion reaction in the MgSO_4 solution is as follows:



Compared with Na_2SO_4 , the formation of ettringite [45] and gypsum is promoted by the interaction of Mg^{2+} and sulfate after MgSO_4 enters the concrete. The erosion product of concrete in MgSO_4 solution is $\text{Mg}(\text{OH})_2$, which changes the pH inside the concrete and transforms the C-S-H to an unbonded C-M-H gel [46,47]. In the upper part of NC-0, needle-rod-like ettringite and massive gypsum can be observed, while in the lower part, small pores filled with ettringite and part of prismatic gypsum can be observed. Compared with the Na_2SO_4 solution, after immersion in the MgSO_4 solution for 180 d, less ettringite and more plate-like crystals were observed in NC-0.

A large amount of ettringite can be observed in the microstructure of RPC-2. In the upper part, the interfacial transition zones between aggregate and mortar had a large amount of reticulated ettringite and sporadic gel, while massive gypsum, ettringite, and part of CH were observed in the lower part. In addition, a large amount of ettringite grew inside the pores of the lower part of the concrete. Besides plate-like CH and prismatic gypsum, ettringite is barely visible in the microstructure of RPC-4. In contrast to the Na_2SO_4 solution, a larger amount of particulate matter was observed in the lower part of RPC-4 immersed in the MgSO_4 solution. The higher the RFP replacement rate, the larger the amount of gypsum produced in the concrete. As a result, the concrete microstructure became looser, and the compressive strength of RPC-4 decreased. Therefore, with higher RFP replacement rates, the RPC is more prone to gypsum-type damage under the combined action of SO_4^{2-} and Mg^{2+} .

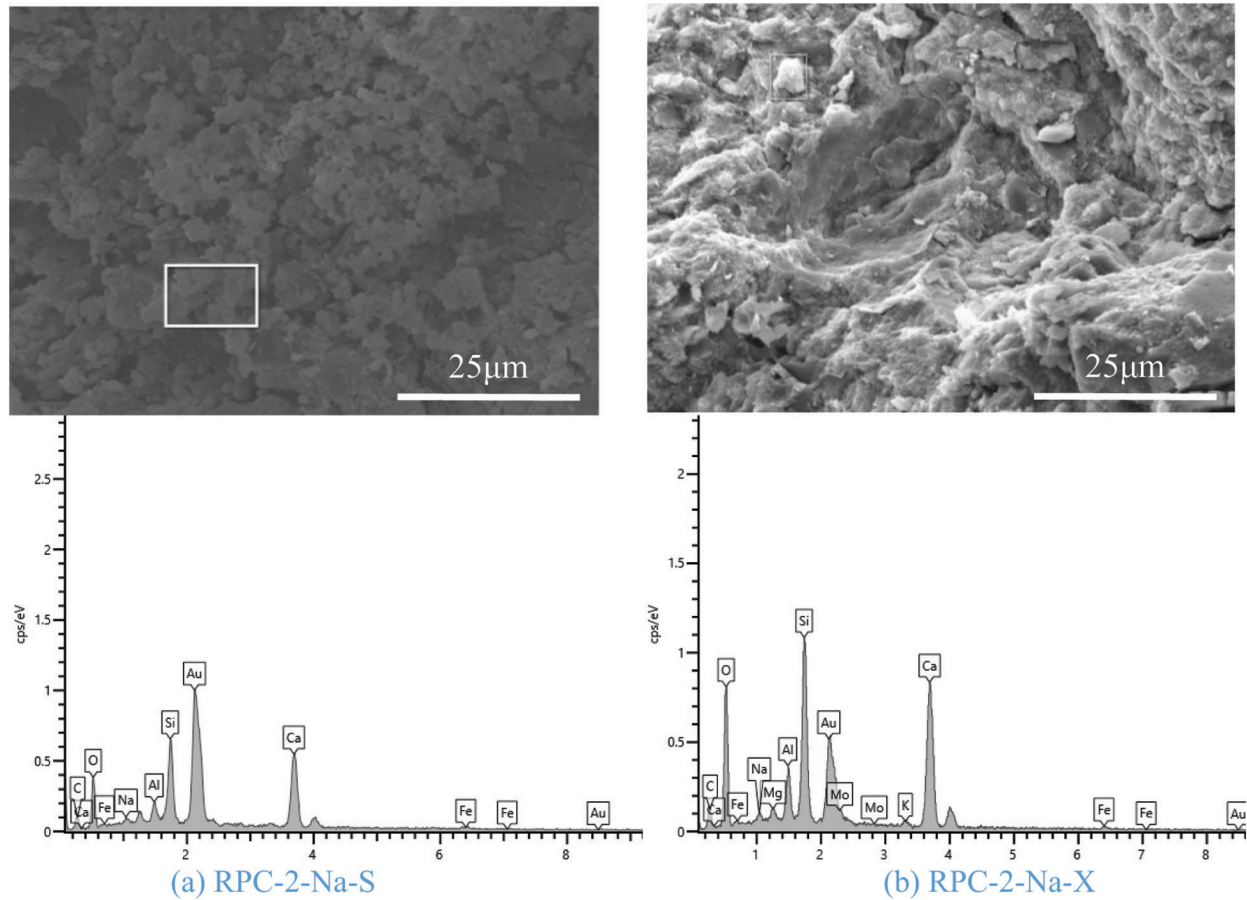


Figure 13: EDS diagrams of the concrete

Note: S represents the upper part of the concrete, X represents the lower part, and 180 d represents the immersion time.

The elemental composition of the microstructure of RPC-2 after the 180 d immersion measured by EDS is shown in Fig. 15. The predominant elements in the upper part of RPC-2 are S, Ca, O, Mg, and S, indicating that the calibrated substances are probably CaSO_4 , gypsum, M-S-H, and thenardite. The large prismatic crystals in the electron micrograph are gypsum, and the small number of granular crystals are thenardite. Therefore, the reaction between MgSO_4 and $\text{Ca}(\text{OH})_2$, chemical erosion, and physical crystallization erosion of MgSO_4 occurred in the upper part of the concrete. The elements in the lower part of RPC-2 are Ca, Si, O, Mg, S, Al, Mg, and C. The peak value of S in the lower part was significantly reduced, and M-S-H, gypsum, and some $\text{Mg}(\text{OH})_2$ may have been produced in the lower part. Eroded by MgSO_4 , the microstructure of RPC-2 changed, and a large amount of gypsum filled its interior. Thus, strong gypsum erosion occurred in the lower part of the concrete.

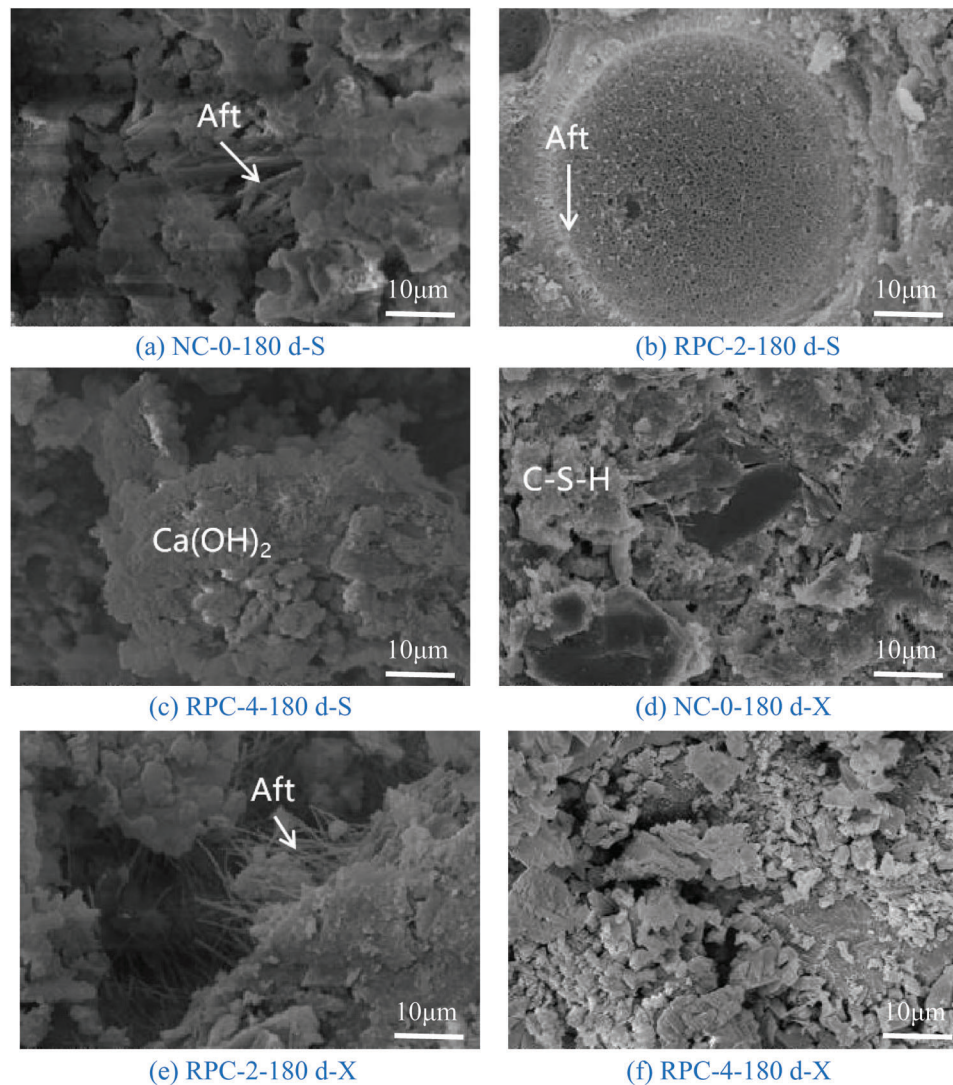


Figure 14: SEM diagram of concrete with different RFP replacement rates $\times 2000$ times

3.7 XRD Analysis

3.7.1 Effect of RFP Replacement Rate on Concrete

To further understand the corrosion products, we performed XRD tests on concrete samples after 180 d of Na_2SO_4 or MgSO_4 immersion. Fig. 16 shows the comparison between the XRD results of RPC-2 and RPC-4. The analysis results show that CaCO_3 , SiO_2 , gypsum, CH, and ettringite are present in the samples after Na_2SO_4 erosion. The contents of gypsum and ettringite (Aft) in RPC-2 were higher than those in RPC-4. The difference between gypsum peaks in RPC-2 and the lower part of RPC-4 is not significant, and the peak Aft of RPC-4 is approximately twice that of RPC-2. After 180 d of Na_2SO_4 erosion, chemical reactions occurred in the upper and lower parts of the concrete to produce gypsum and ettringite, predominantly gypsum. Gypsum erosion was not enhanced with the increase of the RFP replacement rate. Considering the morphology of the concrete, it is safe to conclude that under partial immersion, the upper part of the concrete undergoes internal chemical erosion and physical crystallization on the surface, while the lower part only undergoes chemical erosion. The reason may be that the upper

part has a higher rate of water evaporation due to its contact with air. Thus, the Na_2SO_4 concentration is higher on the surface, and its physical crystallization ensues. In contrast, the lower part is in contact with water, which is not evaporated. Thus, the physical crystallization of Na_2SO_4 on the concrete surface is not possible without a high concentration zone.

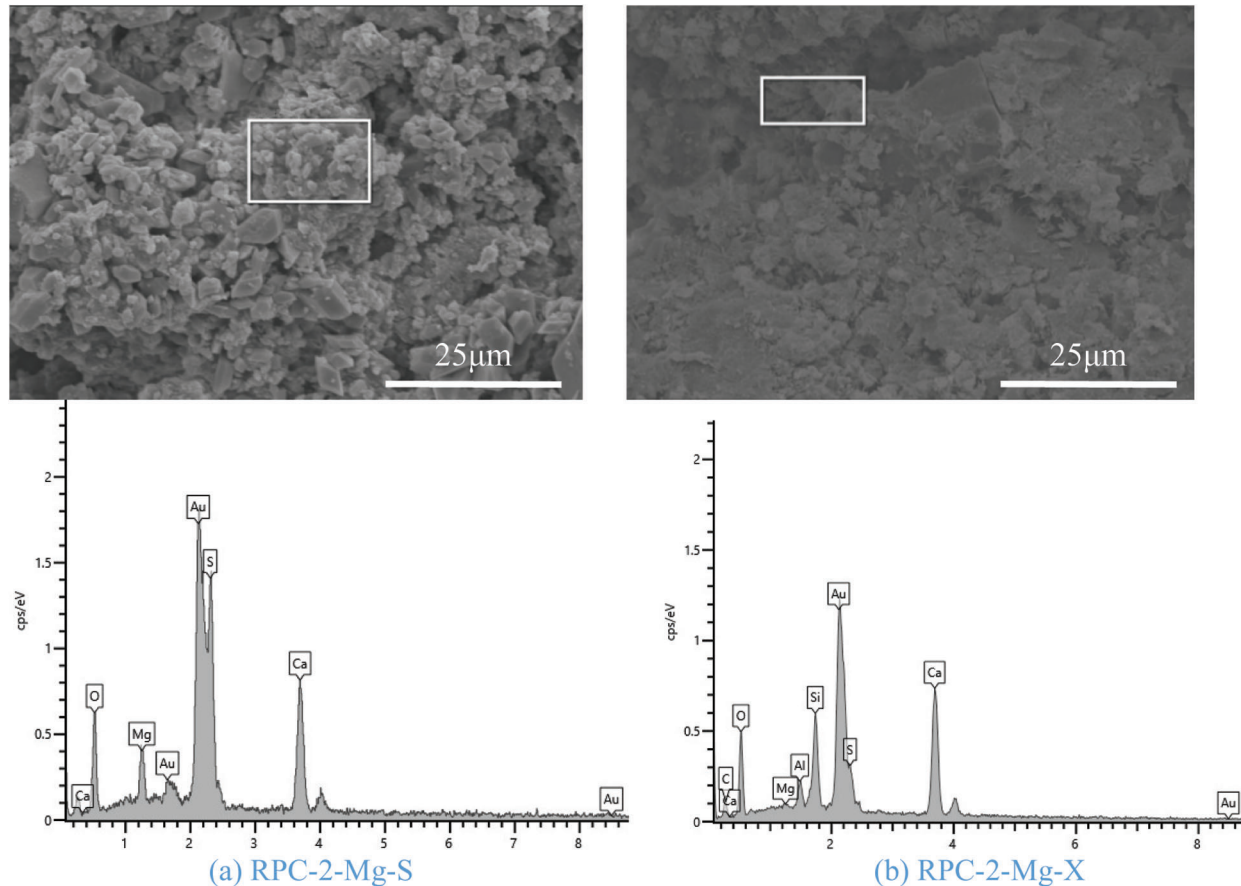


Figure 15: EDS diagram of concrete

After 180 d of partial immersion in MgSO_4 solution, the material composition of the upper and lower parts of the concrete samples is mainly SiO_2 , gypsum, CaCO_3 , CH, and AFt. SiO_2 is mainly derived from the sample containing a certain amount of sand. CaCO_3 is produced by the carbonation of concrete. Gypsum and AFt are the erosion products of concrete attacked by MgSO_4 . The gypsum and calcium alumina diffraction peaks of RPC-2 compared to the upper part of RPC-4. Above the liquid level, the gypsum peak of RPC-4 is higher, but the difference between the peaks of ettringite is not significant, and the pattern is opposite to the results of Na_2SO_4 soaked concrete. At the RFP replacement rate of 40%, MgSO_4 causes more serious chemical erosion in concrete, indicating that a higher RFP replacement rate is more favorable for the reaction between MgSO_4 and RPC. In the lower parts, gypsum and ettringite peaks of RPC-4 were higher than that of RPC-2, and the peak of gypsum in RPC-4 is about 1.5 times that of RPC-2. Therefore, gypsum-based chemical erosion occurred in the upper and lower parts of the RPC immersed in MgSO_4 solution for 180 d. At the concentration of 5%, the chemical reaction between the RPC and MgSO_4 was more intense than that between the RPC and Na_2SO_4 . The reason may be that Mg^{2+} enters the concrete and reacts with it to form $\text{Mg}(\text{OH})_2$, which reduces the pH of RPC. Thus, the decalcification process is

accelerated, resulting in the transition from C-S-H to non-coagulable M-S-H [46,47] and an increase in gypsum production. The results showed that the effects of RFP replacement rate superimposed with the MgSO_4 erosion effects. The higher the RFP replacement rate, the higher the gypsum production.

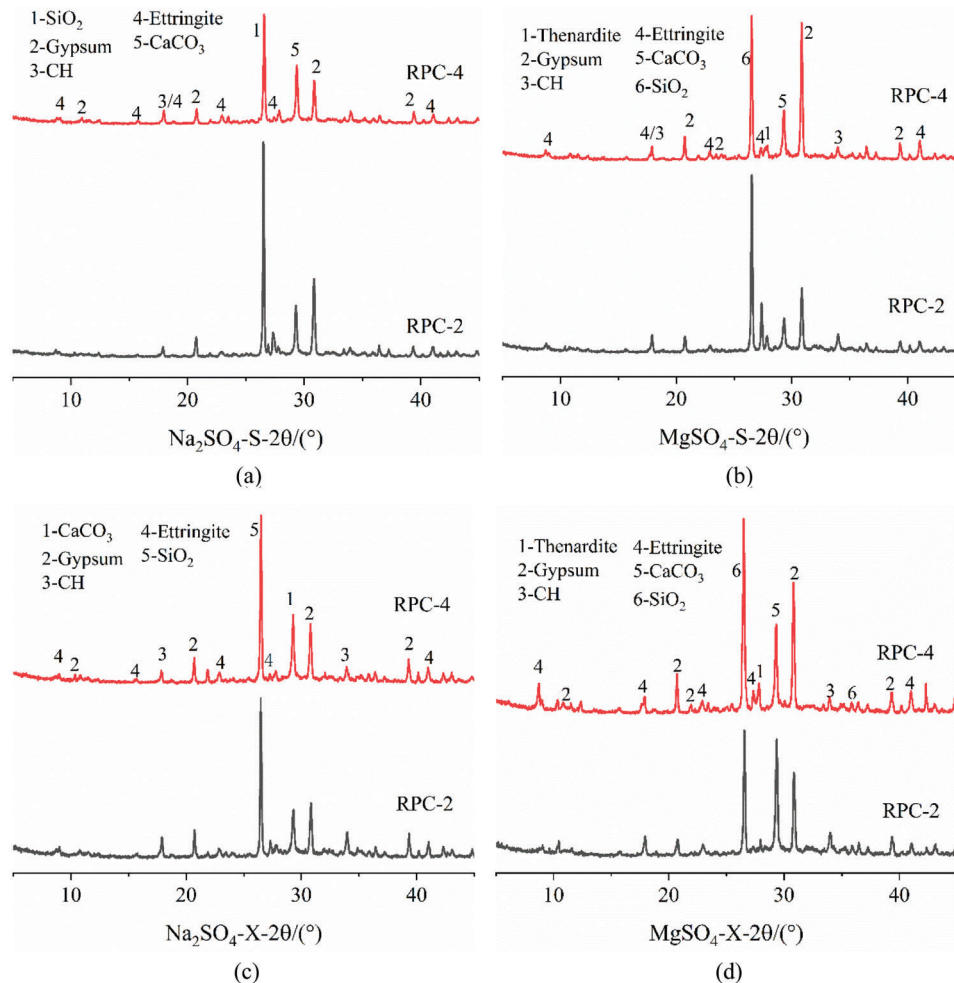


Figure 16: XRD pattern of the concrete

3.7.2 Effect of Immersion Time on Concrete

The XRD results of RPC with 20% RFP immersed in sulfate solutions for 60 and 180 d are shown in Fig. 17. The Na_2SO_4 immersed concrete samples have high SiO_2 diffraction peaks due to the presence of sand. In the upper part, the peak value of gypsum showed limited changes. In the lower part, the peak value of gypsum after 60 d immersion was higher than that after 180 d immersion, and the peak value of ettringite decreased with time. Therefore, the upper part of the concrete immersed in Na_2SO_4 solution undergoes increasingly severe gypsum erosion with the immersion time. However, the amount of ettringite in the lower part of RPC-2 decreased, possibly because the gypsum and ettringite produced in the pre-full immersion period filled the pores on the concrete surface, which led to the reduction of gypsum and ettringite peaks after 180 d.

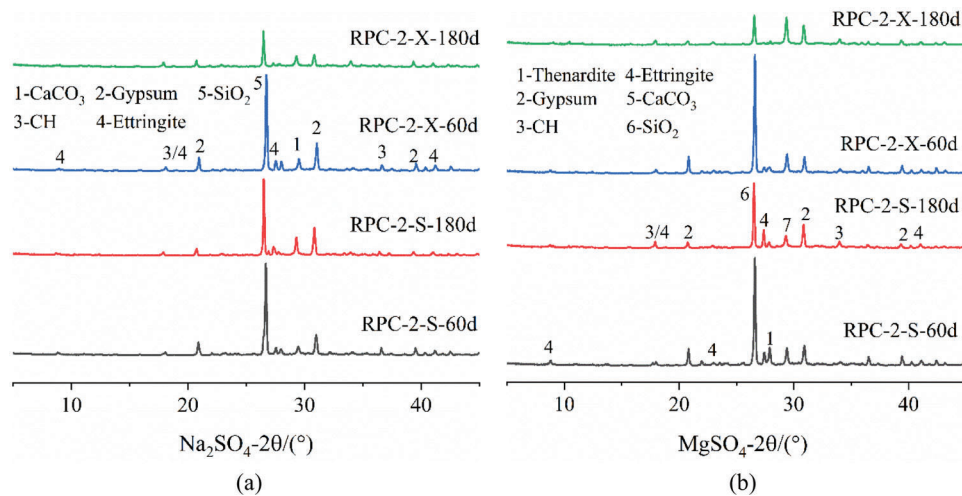


Figure 17: XRD pattern of the concrete

With 20% RFP, the ettringite peak in the upper part of RPC-2 after 180 d of MgSO_4 immersion was slightly higher than that after 60 d of MgSO_4 immersion, but the changes in gypsum were not significant. In the lower parts, the gypsum peak after 60 d immersion was higher than that after 180 d immersion. Therefore, with the increase of immersion time, more ettringite formed in the upper part, i.e., the chemical erosion inside the concrete immersed in MgSO_4 solution produced ettringite. In the lower part, the chemical reaction inside the concrete gradually stabilized in the late stage, and the changes of gypsum and ettringite became limited.

4 Result and Discussion

- (1) After the 180 d of partial immersion in Na_2SO_4 solution, white powder-like crystals were produced in the upper part of the concrete. After the 180 d of partial immersion in MgSO_4 solution, transparent paste-like crystals were produced in the upper part of the concrete. In addition, apparent peeling was observed on the surface of concrete under Na_2SO_4 erosion.
- (2) The compressive strength of ordinary concrete partially immersed in 5% Na_2SO_4 or 5% MgSO_4 solution increased with immersion time. RPC showed different change patterns. The compressive strength in the upper part of the concrete immersed in the Na_2SO_4 solution increased first but decreased before increasing again, while that in the lower part increased first and decreased. The compressive strength in the upper part of the concrete immersed in the MgSO_4 solution showed slight changes, and that in the lower part increased first and then decreased.
- (3) Under sulfate attack, the compressive strength and mass loss rate variation of RPC was relatively limited when the RFP content was below 20%.
- (4) With the increase of RFP replacement rate, the needle-rod crystals decreased, but the block crystals increased. Similar to ordinary concrete, the hydration products were mainly gypsum and ettringite.
- (5) The insides of both the upper and lower parts of RPC were chemically corroded. After being immersed in the Na_2SO_4 solution for 180 d, RFP content showed minor effects on the concrete, and the effects of RFP content superimposed with the MgSO_4 erosion. The higher the RFP content, the more likely the occurrence of gypsum damage.

Acknowledgement: This research was supported by the National Natural Science Foundation of China, Qinghai Provincial Science and Technology Department Basic Research Project and Qinghai Provincial Science and Technology Department Technology Basic Condition Platform Project.

Funding Statement: This research was supported by the National Natural Science Foundation of China (51668052), Qinghai Provincial Science and Technology Department Basic Research Project (2017-ZJ-787) and Qinghai Provincial Science and Technology Department Technology Basic Condition platform Project (2018-ZJ-T01).

Conflicts of Interest: The authors declare that they have no conflicts of interest to report regarding the present study.

References

1. Zhang, P., Wang, K., Wang, J., Guo, J., Hu, S. et al. (2020). Mechanical properties and prediction of fracture parameters of geopolymer/alkali-activated mortar modified with PVA fiber and nano-SiO₂. *Ceramics International*, 46(12), 20027–20037. DOI 10.1016/j.ceramint.2020.05.074.
2. Gao, Z., Zhang, P., Guo, J., Wang, K. (2021). Bonding behavior of concrete matrix and alkali-activated mortar incorporating nano-SiO₂ and polyvinyl alcohol fiber: Theoretical analysis and prediction model. *Ceramics International*, 47(22), 31638–31649. DOI 10.1016/j.ceramint.2021.08.044.
3. Revilla-Cuesta, V., Ortega-López, V., Skaf, M., Manso, J. M. (2020). Effect of fine recycled concrete aggregate on the mechanical behavior of self-compacting concrete. *Construction and Building Materials*, 263, 120671. DOI 10.1016/j.conbuildmat.2020.120671.
4. Xiao, J., Ma, Z., Sui, T., Akbarnezhad, A., Duan, Z. (2018). Mechanical properties of concrete mixed with recycled powder produced from construction and demolition waste. *Journal of Cleaner Production*, 188, 720–731. DOI 10.1016/j.jclepro.2018.03.277.
5. Duan, Z., Singh, A., Xiao, J., Hou, S. (2020). Combined use of recycled powder and recycled coarse aggregate derived from construction and demolition waste in self-compacting concrete. *Construction and Building Materials*, 254, 119323. DOI 10.1016/j.conbuildmat.2020.119323.
6. Evangelista, L., Guedes, M., de Brito, J., Ferro, A. C., Pereira, M. F. (2015). Physical, chemical and mineralogical properties of fine recycled aggregates made from concrete waste. *Construction and Building Materials*, 86, 178–188. DOI 10.1016/j.conbuildmat.2015.03.112.
7. Poon, C. S., Chan, D. (2006). Feasible use of recycled concrete aggregates and crushed clay brick as unbound road sub-base. *Construction and Building Materials*, 20(8), 578–585. DOI 10.1016/j.conbuildmat.2005.01.045.
8. Herrador, R., Pérez, P., Garach, L., Ordóñez, J. (2012). Use of recycled construction and demolition waste aggregate for road course surfacing. *Journal of Transportation Engineering*, 138(2), 182–190. DOI 10.1061/(ASCE)TE.1943-5436.0000320.
9. Xuan, D. X., Molenaar, A. A. A., Houben, L. J. M. (2016). Shrinkage cracking of cement treated demolition waste as a road base. *Materials and Structures*, 49(1), 631–640. DOI 10.1617/s11527-015-0524-7.
10. Li, Y., Wang, R., Li, S., Zhao, Y., Qin, Y. (2018). Resistance of recycled aggregate concrete containing low- and high-volume fly ash against the combined action of freeze–thaw cycles and sulfate attack. *Construction and Building Materials*, 166, 23–34. DOI 10.1016/j.conbuildmat.2018.01.084.
11. Wang, R., Yu, N., Li, Y. (2020). Methods for improving the microstructure of recycled concrete aggregate: A review. *Construction and Building Materials*, 242, 118164. DOI 10.1016/j.conbuildmat.2020.118164.
12. Irki, I., Debieb, F., Ouzadid, S., Dilmi, H. L., Settari, C. et al. (2018). Effect of blaine fineness of recycling brick powder replacing cementitious materials in self compacting mortar. *Journal of Adhesion Science and Technology*, 32(9), 963–975. DOI 10.1080/01694243.2017.1393202.
13. Duan, Z., Hou, S., Xiao, J., Li, B. (2020). Study on the essential properties of recycled powders from construction and demolition waste. *Journal of Cleaner Production*, 253, 119–865. DOI 10.1016/j.jclepro.2019.119865.

14. Tang, Q., Ma, Z., Wu, H., Wang, W. (2020). The utilization of eco-friendly recycled powder from concrete and brick waste in new concrete: A critical review. *Cement and Concrete Composites*, 114, 103807. DOI 10.1016/j.cemconcomp.2020.103807.
15. Oksri-Nelfia, L., Mahieux, P. Y., Amiri, O., Turcry, P., Lux, J. (2016). Reuse of recycled crushed concrete fines as mineral addition in cementitious materials. *Materials and Structures*, 49(8), 3239–3251. DOI 10.1617/s11527-015-0716-1.
16. Neville, A. (2004). The confused world of sulfate attack on concrete. *Cement and Concrete Research*, 34(8), 1275–1296. DOI 10.1016/j.cemconres.2004.04.004.
17. Tian, B., Cohen, M. D. (2000). Does gypsum formation during sulfate attack on concrete lead to expansion? *Cement and Concrete Research*, 30(1), 117–123. DOI 10.1016/S0008-8846(99)00211-2.
18. Rozière, E., Loukili, A., El Hachem, R., Grondin, F. (2009). Durability of concrete exposed to leaching and external sulphate attacks. *Cement and Concrete Research*, 39(12), 1188–1198. DOI 10.1016/j.cemconres.2009.07.021.
19. Santhanam, M., Cohen, M. D., Olek, J. (2001). Sulfate attack research—whither now? *Cement and Concrete Research*, 31(6), 845–851. DOI 10.1016/S0008-8846(01)00510-5.
20. Chen, J. K., Jiang, M. Q. (2009). Long-term evolution of delayed ettringite and gypsum in portland cement mortars under sulfate erosion. *Construction and Building Materials*, 23(2), 812–816. DOI 10.1016/j.conbuildmat.2008.03.002.
21. Ikumi, T., Cavalaro, S. H., Segura, I., de la Fuente, A., Aguado, A. (2016). Simplified methodology to evaluate the external sulfate attack in concrete structures. *Materials & Design*, 89, 1147–1160. DOI 10.1016/j.matdes.2015.10.084.
22. Liu, P., Chen, Y., Wang, W., Yu, Z. (2020). Effect of physical and chemical sulfate attack on performance degradation of concrete under different conditions. *Chemical Physics Letters*, 745, 137254. DOI 10.1016/j.cplett.2020.137254.
23. Zhang, Z., Jin, X., Luo, W. (2019). Long-term behaviors of concrete under low-concentration sulfate attack subjected to natural variation of environmental climate conditions. *Cement and Concrete Research*, 116, 217–230. DOI 10.1016/j.cemconres.2018.11.017.
24. Komljenović, M., Baščarević, Z., Marjanović, N., Nikolić, V. (2013). External sulfate attack on alkali-activated slag. *Construction and Building Materials*, 49, 31–39. DOI 10.1016/j.conbuildmat.2013.08.013.
25. Guo, L., Wu, Y., Duan, P., Zhang, Z. (2020). Improving sulfate attack resistance of concrete by using calcined Mg-Al-CO₃ LDHs: Adsorption behavior and mechanism. *Construction and Building Materials*, 232, 117–256. DOI 10.1016/j.conbuildmat.2019.117256.
26. Nehdi, M. L., Suleiman, A. R., Soliman, A. M. (2014). Investigation of concrete exposed to dual sulfate attack. *Cement and Concrete Research*, 64, 42–53. DOI 10.1016/j.cemconres.2014.06.002.
27. Wu, M., Zhang, Y., Ji, Y., She, W., Yang, L. et al. (2020). A comparable study on the deterioration of limestone powder blended cement under sodium sulfate and magnesium sulfate attack at a low temperature. *Construction and Building Materials*, 243, 118–279. DOI 10.1016/j.conbuildmat.2020.118279.
28. Xiong, C., Jiang, L., Xu, Y., Song, Z., Chu, H. et al. (2016). Influences of exposure condition and sulfate salt type on deterioration of paste with and without fly ash. *Construction and Building Materials*, 113, 951–963. DOI 10.1016/j.conbuildmat.2016.03.154.
29. Ogawa, Y., Bui, P. T., Kawai, K., Sato, R. (2020). Effects of porous ceramic roof tile waste aggregate on strength development and carbonation resistance of steam-cured fly ash concrete. *Construction and Building Materials*, 236, 117–462. DOI 10.1016/j.conbuildmat.2019.117462.
30. Nie, Q., Zhou, C., Li, H., Shu, X., Gong, H. et al. (2015). Numerical simulation of fly ash concrete under sulfate attack. *Construction and Building Materials*, 84, 261–268. DOI 10.1016/j.conbuildmat.2015.02.088.
31. Deng, G., He, Y., Lu, L., Hu, S. (2020). Evolution of aluminate hydrate phases in fly ash-cement system under the sulfate conditions. *Construction and Building Materials*, 252, 119045. DOI 10.1016/j.conbuildmat.2020.119045.
32. Džunuzović, N., Komljenović, M., Nikolić, V., Ivanović, T. (2017). External sulfate attack on alkali-activated fly ash-blast furnace slag composite. *Construction and Building Materials*, 157, 737–747. DOI 10.1016/j.conbuildmat.2017.09.159.

33. Jiang, C., Jiang, L., Li, S., Tang, X., Zhang, L. (2021). Impact of cation type and fly ash on deterioration process of high belite cement pastes exposed to sulfate attack. *Construction and Building Materials*, 286, 122961. DOI 10.1016/j.conbuildmat.2021.122961.
34. Chen, X., Li, Y., Bai, H., Ma, L. (2021). Utilization of recycled concrete powder in cement composite: Strength, microstructure and hydration characteristics. *Journal of Renewable Materials*, 9(12), 2189–2208. DOI 10.32604/jrm.2021.015394.
35. GB/T 50081-2019 (2019). Standard for test methods for physical and mechanical properties of concrete. Beijing, China: Standardization Administration of China.
36. Pel, L., Huinink, H., Kopinga, K. (2003). Salt transport and crystallization in porous building materials. *Magnetic Resonance Imaging*, 21(3–4), 317–320. DOI 10.1016/S0730-725X(03)00161-9.
37. Pel, L., Huinink, H., Kopinga, K., van Hees, R. P. J., Adan, O. C. G. (2004). Efflorescence pathway diagram: Understanding salt weathering. *Construction and Building Materials*, 18(5), 309–313. DOI 10.1016/j.conbuildmat.2004.02.003.
38. Al-Amoudi, O. S. B., Maslehuddin, M., Saadi, M. M. (1995). Effect of magnesium sulfate and sodium sulfate on the durability performance of plain and blended cements. *ACI Materials Journal*, 92(1), 15–24. DOI 10.14359/1173.
39. Liu, Z., Deng, D., de Schutter, G., Yu, Z. (2012). Chemical sulfate attack performance of partially exposed cement and cement + fly ash paste. *Construction and Building Materials*, 28(1), 230–237. DOI 10.1016/j.conbuildmat.2011.08.071.
40. Wang, K., Guo, J., Wu, H., Yang, L. (2020). Influence of dry-wet ratio on properties and microstructure of concrete under sulfate attack. *Construction and Building Materials*, 263, 120635. DOI 10.1016/j.conbuildmat.2020.120635.
41. Gao, R., Li, Q., Zhao, S. (2013). Concrete deterioration mechanisms under combined sulfate attack and flexural loading. *Journal of Materials in Civil Engineering*, 25(1), 39–44. DOI 10.1061/(ASCE)MT.1943-5533.0000538.
42. He, R., Zheng, S., Gan, V. J., Wang, Z., Fang, J. et al. (2020). Damage mechanism and interfacial transition zone characteristics of concrete under sulfate erosion and dry-wet cycles. *Construction and Building Materials*, 255, 119340. DOI 10.1016/j.conbuildmat.2020.119340.
43. Zhao, G., Guo, M., Cui, J., Li, J., Xu, L. (2021). Partially-exposed cast-in-situ concrete degradation induced by internal-external sulfate and magnesium multiple coupled attack. *Construction and Building Materials*, 294, 123560. DOI 10.1016/j.conbuildmat.2021.123560.
44. Rasheeduzzafar, Al-Amoudi O. S. B., Abduljawwad, S. N., Maslehuddin, M. (1994). Magnesium-sodium sulfate attack in plain and blended cements. *Journal of Materials in Civil Engineering*, 6(2), 201–222. DOI 10.1061/(ASCE)0899-1561(1994)6:2(201).
45. Yu, C., Sun, W., Scrivener, K. (2013). Mechanism of expansion of mortars immersed in sodium sulfate solutions. *Cement and Concrete Research*, 43, 105–111. DOI 10.1016/j.cemconres.2012.10.001.
46. Santhanam, M., Cohen, M. D., Olek, J. (2002). Mechanism of sulfate attack: A fresh look: Part 1: Summary of experimental results. *Cement and Concrete Research*, 32(6), 915–921. DOI 10.1016/S0008-8846(02)00724-X.
47. Santhanam, M., Cohen, M. D., Olek, J. (2003). Mechanism of sulfate attack: A fresh look: Part 2. Proposed mechanisms. *Cement and Concrete Research*, 33(3), 341–346. DOI 10.1016/S0008-8846(02)00958-4.